CERN Summer Student Programme 2019

Individual Report

Studies for a New Trigger for the Measurement of the Weak Mixing Angle with the ATLAS Detector

Supervised by:
Daniele Zanzi
Alexis Vallier

Submitted by :
Yens Killian Elskens

Contents

1 Introduction

Particle physics has undergone a revolution throughout the last 100 years. Since the early 1950's, the European Organization for Nuclear Research (CERN) has played a major role in this revolution, using state-of-the-art detection techniques. Possessing now since 2007 the world's largest and most powerful accelerator (the Large Hadron Collider, LHC), CERN owns one of the most precious tools used in the pursue of understanding the Universe. The LHC consists of a large ring with a 27 km circumference of superconducting magnets, colliding protons at an energy of 13 TeV at four different interaction points.

At one of these four collision points, the ATLAS experiment is located. It is a general-purpose particle physics experiment and is designed to exploit the full discovery potential and the huge range of physics opportunities that the LHC provides [1].

During the run 2 of the LHC there occurred up to 1.7 billion collisions per second at the ATLAS detector [2]. Since it is not possible to store all this data for further analysis, over 99% of the data is almost immediately discarded. In order to ensure that no interesting data is lost during this process a trigger system is required. The ATLAS trigger system will carry out the selection process in two stages: the Level-1 (L1) trigger, which will select data based on information from the calorimeter and muon detectors and saves at most around 100 000 events each second, and the High-Level Trigger (HLT), which consists of a large farm of CPUs which refines the analysis of the L1 trigger, and selects about 1000 events per second to be passed on to data storage [2].

This report will focus on proposed upgrades for a trigger whose objective is to improve the accuracy on measurements of the weak mixing angle for run 3 of the LHC. A motivation for this search and the experimental implications will be covered in section 2, an analysis of the efficiency and possible optimizations of the run 3 trigger proposal will be discussed in sections 3.1 and 3.2 respectively. Finally, a conclusion will be provided in section 4.

2 Motivation

2.1 Theoretical Motivation

The weak mixing angle is a very important parameter in the Standard Model of Particle Physics. It is the angle which rotates the original B_μ (arising from the $U(1)_Y$ gauge symmetry) and W_μ^3 (arising from the $SU(2)_L$ gauge symmetry) vector boson fields to produce the Z-boson and the photon through the mechanism of spontaneous symmetry breaking. At tree level, it relates the mass of the W-boson to the mass of the Z-boson via [3]

$$\cos\theta_W = \frac{M_Z}{M_W}\,, \tag{1a}$$

$$\sin^2\theta_W = 1 - \left(\frac{M_W}{M_Z}\right)^2\,. \tag{1b}$$

The weak mixing angle thus plays a key role in understanding the Brout-Englert-Higgs mechanism and, through this, the Standard Model itself.

In order to test the consistency of the Standard Model, its parameters need to be measured precisely and compared with SM predictions, and a common thing to do is plotting the contours of the 68% and 95% confidence levels of M_W and $\sin^2\theta_W$ measurements, as can be seen in Figure 1. Here the green contours represent

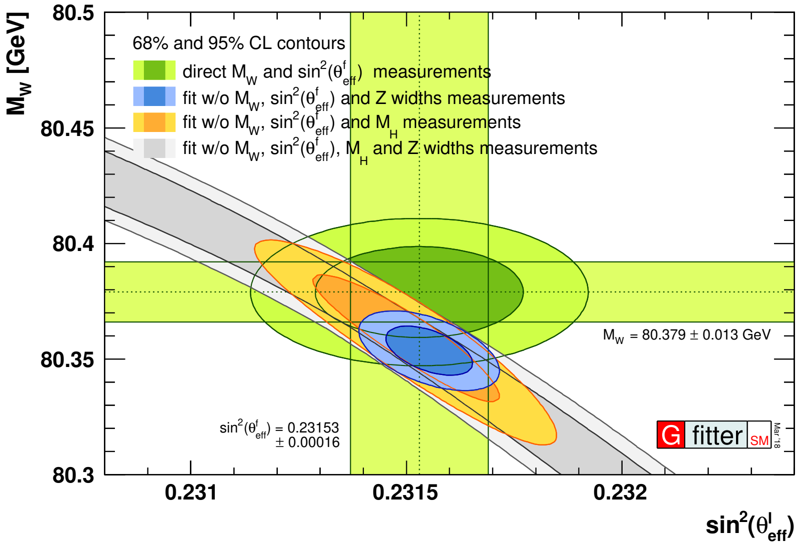

Figure 1: Contours at 68% and 95% confidence level obtained from a global fit of SM parameters without including M_W and $\sin^2\theta_{\text{eff}}$ measurements. Horizontal bands indicate 1σ regions on direct measurements [4].

direct measurements, while the blue contours represent fits of M_W and $\sin^2\theta_W$ by assuming the SM predictions and using all the measurements of its other free parameters (except for the Z-width) as constraints. Given the current precision, SM predictions are in good agreement with the direct measurements. There have been, however, observations of certain phenomena which are not described by the Standard Model (such as the flatness of rotation curves of spiral galaxies at high radii, matter-antimatter asymmetry in the Universe, neutrino masses. . .) which strongly support the idea of its incompleteness. Performing direct measurements of the weak mixing angle with a higher accuracy could therefore decrease the size of the green ellipse in Figure 1 such that the fit may no longer be consistent with the direct measurements.

Experimentally, the weak mixing angle can be inferred from the $q\bar{q} \to \ell\bar{\ell}$ process whose cross section can be decomposed in harmonic polynomials. Each of these harmonic polynomials will possess a so-called angular coefficient, A_i, and at leading order (LO) only the fourth angular coefficient is non-zero, for which the cross section then becomes [5]

$$\frac{\mathrm{d}\sigma}{\mathrm{d}y_{\ell\ell}\,\mathrm{d}m_{\ell\ell}\,\mathrm{d}\cos\theta} = \frac{3}{16\pi}\frac{\mathrm{d}\sigma^{U+L}}{\mathrm{d}y_{\ell\ell}\,\mathrm{d}m_{\ell\ell}}\left\{(1+\cos^2\theta) + A_4\cos\theta\right\} \tag{2}$$

where σ^{U+L} represents the unpolarized cross section, $y_{\ell\ell}$ is the rapidity and $m_{\ell\ell}$ the invariant mass of the dileptonic system. Here θ represents the polar angle in the Collins-Soper (CS) frame. The leading order Feynman diagram for this process can be found in Figure 2. In equation (2) the A_4 coefficient depends on the product of vector and axial couplings to fermions and is sensitive to the weak mixing angle [5]. In short, in order to increase the accuracy on direct measurements of the weak mixing

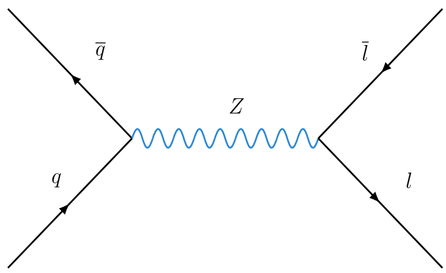

Figure 2: Leading order (LO) Feynman diagram of the $q\bar{q} \to \ell\bar{\ell}$ Drell-Yan process.

angle, one needs to increase the accuracy on the A_4 measurements. Following this logic, it can be seen from Figure 3, which represents the theoretical A_4 predictions in function of the rapidity of the dileptonic system, that high $y_{\ell\ell}$ measurements would increase the statistical significance of an A_4 measurement, which would thus lead to more precise measurements of the weak mixing angle. This is because high $y_{\ell\ell}$ correspond to a Z-boson which is highly boosted, such that the interacting quark direction is well known [6].

In other words, events where the produced Z-boson has a very high rapidity are very coveted for optimizing weak mixing angle measurements. The ATLAS detector can reconstruct $Z \to \ell\ell$ events at high $y_{\ell\ell}$ when the Z-boson decays to electrons thanks to the ATLAS forward calorimeters. The purpose of this study is therefore to improve the acceptance of the forward $Z \to ee$ events with a new trigger to improve the measurement of the weak mixing angle.

2.2 Experimental Implications

Events where the produced Z-boson has such a high rapidity usually have at least one "forward electron" (denoted as e_F), i.e. an electron with such a high pseudorapidity that it will not go through the tracker, but will only be detected in the calorimeter, as opposed to a "central electron" (denoted as e_C), which does pass through the tracker.

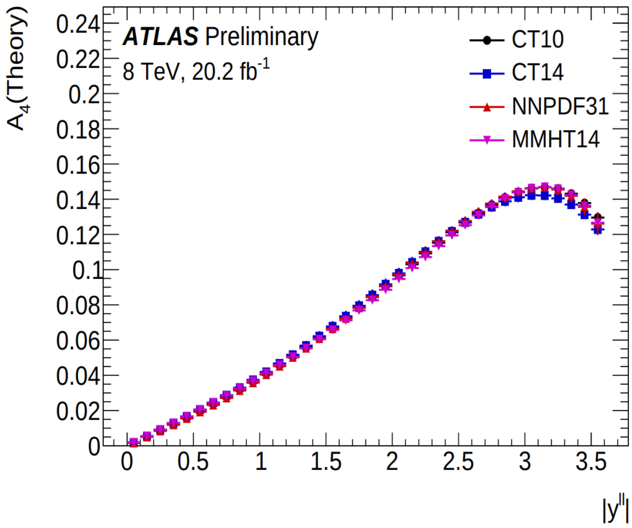

Figure 3: A_4 prediction in function of the rapidity of the reconstructed dileptonic system [5].

This can be seen from Figure 4 where the green curve represents the number of expected events where the Z-boson decayed into one central and one forward electron. Even though the expected number of events in this rapidity region is much lower

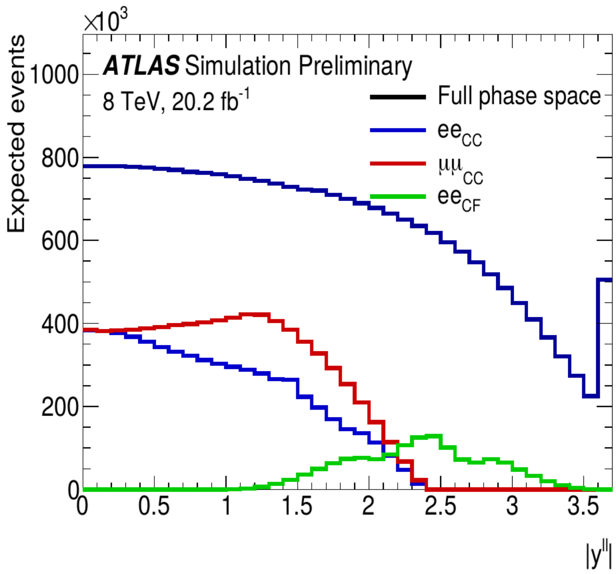

Figure 4: Expected Z-boson signal events as a function of $|y_{\ell\ell}|$ for the ee_{CC}, $\mu\mu_{CC}$ and ee_{CF} channels. Copied from [5].

than, for example, events where two central electrons are produced, the sensitivity gain one gets from looking to high rapidity events has a much larger influence on the accuracy of the weak mixing angle measurement, as can be seen in Figure 5, which shows different measurements of the weak mixing angle for different experiments and their corresponding uncertainties. In order, then, to be able to optimize the acceptance of events which are significant to high precision measurements of the weak mixing angle, a trigger on central-forward events should be constructed.

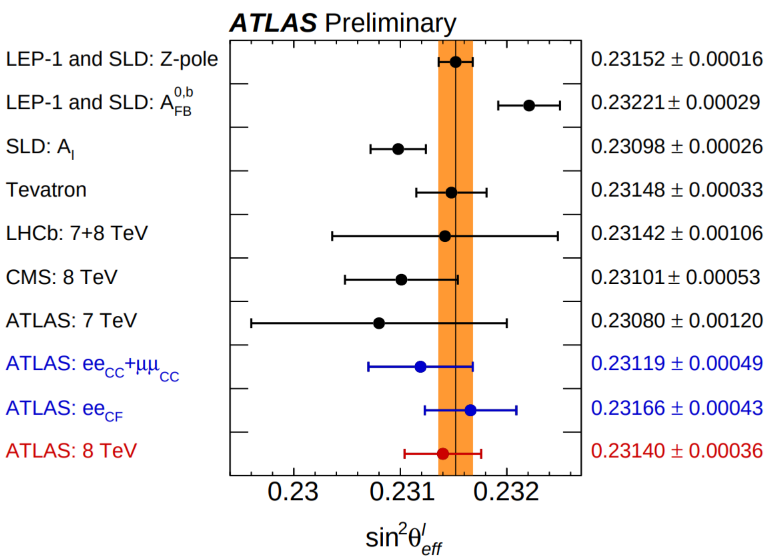

Figure 5: Comparison of measurements of the weak mixing angle [5].

The trigger at ATLAS during run 1 and 2 of the LHC solely triggered the CF-events on properties concerning the central electron, while exerting two offline cuts on the transverse momentum of both electrons, as schematically shown in Figure 6a. In order to increase the accuracy on weak mixing angle measurements, one can accept more CF-events by lowering the p_T-cut on the central electron (as shown in Figure 6b) and, in order to be able to deal with the increase in rate, further add a trigger selection on properties concerning the dileptonic system (such as the azimuthal angle difference $\Delta\phi_{\ell\ell}$ and the invariant mass $m_{\ell\ell}$).

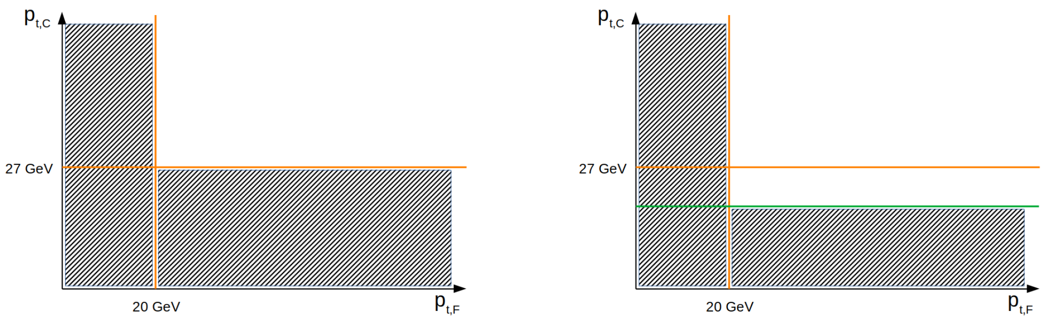

(a) Offline p_T-cuts at run 1 & 2.

(b) Proposal for offline p_T-cuts for run 3.

Figure 6: Schematic view of the offline p_T-cuts used during run 1 and 2 compared to the proposal for run 3.

3 Analysis

3.1 Testing the New Trigger Proposal

As mentioned in the previous section, during the previous two runs of the LHC, the ATLAS trigger for CF was based only on the detection of the central electron. It implied a rather high offline p_T-cut. More specifically, this L1 trigger consisted of a transverse energy cut of $E_{T,0}^{L1} > 22\,\text{GeV}$ (properties measured for the central electron are denoted with a 0 in the subscript, while properties measured for the forward electron are denoted with a 1 in the subscript) as well as a pseudorapidity cut of $|\eta_{\ell,0}^{L1}| < 2.5$ and an isolation cut. This L1 trigger has been labeled `L1_EM22VHI` and is followed by an offline cut on the central electron of $p_{T,0} > 27\,\text{GeV}$ (as shown in Figure 6a). There are selections also at the HLT, but these are not relevant for this study since the acceptance of the CF events is primarily driven by the selections at L1.

At L1, the trigger proposal for run 3 will have a lower p_T-cut on the central electron and in order to be able to handle the rate increase, following online cuts are proposed

- Transverse energy cuts on both the central and the forward electron
  - $E_{T,0}^{L1} \geqslant 18\,\text{GeV}$
  - $E_{T,1}^{L1} \geqslant 15\,\text{GeV}$
- A pseudorapidity cut on the forward electron of $2.3 < |\eta_{\ell,1}^{L1}| < 4.9$
- An invariant mass cut of $m_{\ell\ell}^{L1} > 60\,\text{GeV}$
- An azimuthal angle difference cut of $2.5\,\text{rad} \leqslant \Delta\phi_{\ell\ell}^{L1} \leqslant 3.2\,\text{rad}$

This L1 trigger proposal for run 3 has been labeled `L1_ZAFB-25DPHI-EM18I` and events collected by this new trigger are expected to be analyzed with an offline cut on the central electron of $p_{T,0} > 21\,\text{GeV}$ and on the forward electron of $p_{T,1} > 20\,\text{GeV}$ (as shown in Figure 6b).

Independent of the used L1 trigger, all events also undergo a baseline offline selection, which contains following cuts

- Pseudorapidity cuts on both the central and forward electron
  - $|\eta_{\ell,0}| < 2.4$
  - $2.5 < |\eta_{\ell,1}| < 4.9$ and $|\eta_{\ell,1}| \notin \,]3.1, 3.35[$
- Transverse momentum cut on both the central and the forward electron of $p_{T,0}, p_{T,1} > 20\,\text{GeV}$

In order to observe the effects of this new trigger proposal, it can be applied to a run 2 simulation and compared with both the previous L1 trigger and the shared offline cuts. In order to quantify the possible gain of the new trigger proposal with respect to the old trigger, the ratio between the number of accepted events by each L1 trigger and the baseline offline selection needs to be calculated. In other words, the efficiency of both triggers can be quantified as follows

$$\varepsilon_{\text{new}} = \frac{\#\,\text{events accepted by the new trigger proposal+corresponding offline } p_T\text{-cuts}}{\#\,\text{events accepted by the baseline offline selection}}, \tag{3a}$$

$$\varepsilon_{\text{old}} = \frac{\#\,\text{events accepted by the old trigger+corresponding offline } p_T\text{-cuts}}{\#\,\text{events accepted by the baseline offline selection}}. \tag{3b}$$

The effects of the triggers on dileptonic properties ($\Delta\phi_{\ell\ell}, p_{T,\ell\ell}, m_{\ell\ell}, y_{\ell\ell}$) and their respective efficiencies can be viewed in Figure 7 where the solid red line represents the baseline offline selection, the solid blue line represents the old trigger selection (L1_EM22VHI+offline selections) and the dashed purple line is the new trigger selection (L1_ZAFB-25DPHI-EM18+offline selections).

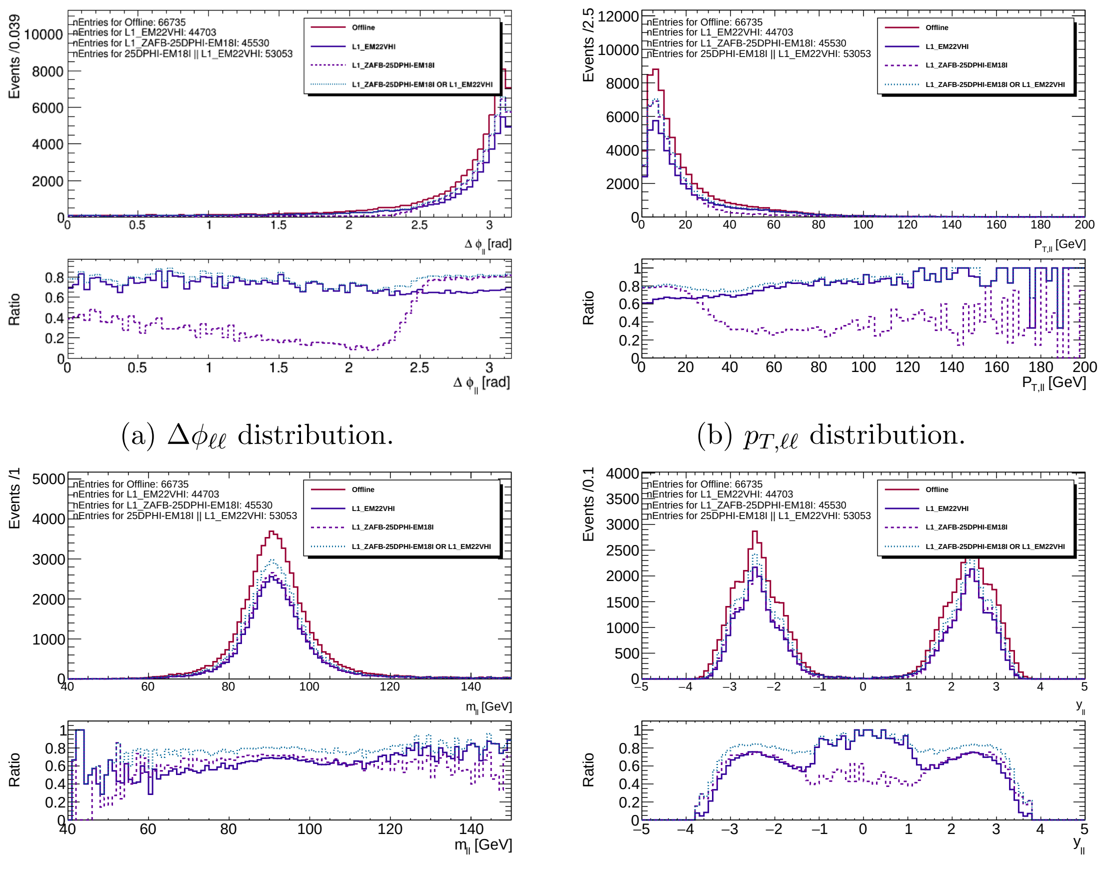

(a) $\Delta\phi_{\ell\ell}$ distribution.

(b) $p_{T,\ell\ell}$ distribution.

(c) $m_{\ell\ell}$ distribution.

(d) $y_{\ell\ell}$ distribution.

Figure 7: Comparing the effects of the old (solid blue) and new (dashed purple) L1 trigger on distributions of dileptonic properties to the baseline offline selection (solid red).

In Figure 7a the online $\Delta\phi_{\ell\ell}^{L1}$ selection can be seen through an efficiency drop of the new proposal when going to angle differences smaller than 2.5 rad, while having a higher efficiency than the old trigger at large angle differences. Since generally high-$p_{T,\ell\ell}$ events correspond to small $\Delta\phi_{\ell\ell}$, a similar efficiency drop can be seen in Figure 7b when going from low to high $p_{T,\ell\ell}$.

In order to obtain a maximum efficiency over all regions, both the old trigger and new trigger proposal are combined: either an event satisfies the old trigger of it satisfies the new proposal (or both), which is represented in the plots of Figure 7 by the dotted light blue line. The efficiency is then quantified as

$$\varepsilon_{\text{old}||\text{new}} = \frac{\#\,\text{events accepted by either the old or the new trigger or both}}{\#\,\text{events accepted by the baseline offline selection}}\,. \tag{4}$$

When calculating this efficiency it was found that there was an overall increase of 12.5%, while when looking at the low $p_{T,\ell\ell}$ regions (i.e. $p_{T,\ell\ell} < 20\,\text{GeV}$), an efficiency increase of 15.1% is observed.

It can thus be concluded that the new trigger proposal, being used in combination with the original trigger, increases in overall efficiency.

3.2 Optimizing the New Trigger Proposal

One can now ask the question whether this new proposal is optimal. In order to do so the new trigger proposal was reconstructed by matching level-1 objects with the offline objects according to minimizing the ΔR defined as

$$\Delta R = \sqrt{\Delta\phi^2 + \Delta\eta^2}\,, \tag{5}$$

where $\Delta\phi$ (resp. $\Delta\eta$) represents, in this case, the azimuthal angle difference (resp. pseudorapidity difference) between the considered L1 object and the offline object. In this way, the most probable L1 candidate corresponding to the offline measurement can be found and based on those findings, L1 selections can be implemented and altered. The distributions corresponding to these L1-measurements can be found in Appendix B.

As a sanity check the effects of the reconstructed new trigger proposal (from now on labeled as `myL1_ZAFB-25DPHI-EM18`) on dynamical properties can be compared to observed effects of the original new trigger proposal. These effects on the distributions of observables concerning the dileptonic system can be seen in Figure 8. In these plots the dashed green curve represents the effect of the reconstructed new proposal while the dotted lighter green curve represents the effects of the original new proposal. The solid light blue (resp. dark blue line) represents the effects of the offline selection (resp. old trigger).

It can be noticed that histograms of the original and reconstructed new trigger proposal don't coincide everywhere. In the $\Delta\phi_{\ell\ell}$ distribution in Figure 8a at high values the reconstructed trigger accepts more events; this is due to the fact that the original also includes a selection on the isolation of the detected object, which was not taken into account during the reconstruction. At lower $\Delta\phi_{\ell\ell}$ values, on the other

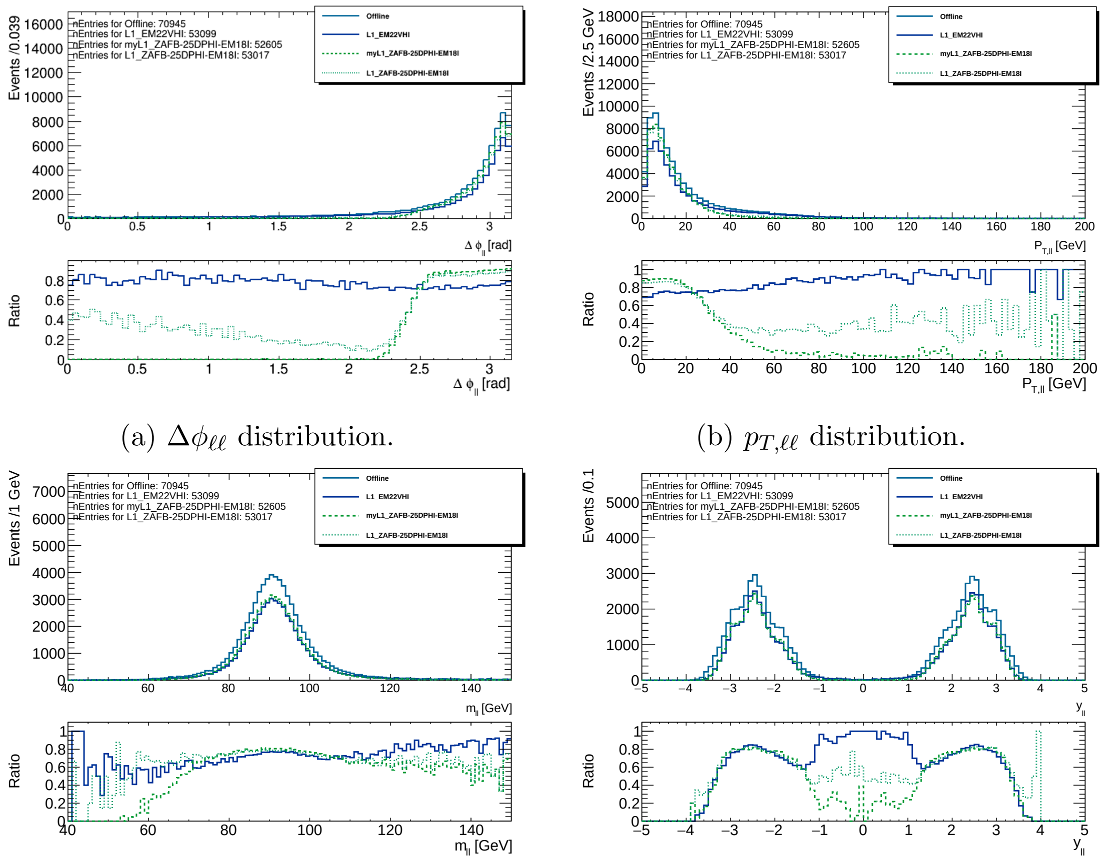

(a) $\Delta\phi_{\ell\ell}$ distribution.

(b) $p_{T,\ell\ell}$ distribution.

(c) $m_{\ell\ell}$ distribution.

(d) $y_{\ell\ell}$ distribution.

Figure 8: Comparing the effects of the reconstructed (dashed green) on distributions of dileptonic properties to the original (dotted green) new L1 trigger.

hand, the original proposal accepts more events. This can be explained by the fact that the original new trigger was constructed by accepting any two objects that pass the L1-trigger, which are not necessarily two electrons (but, for example, an electron and a jet) while the reconstructed trigger was constructed by only looking at electrons and matching the L1 objects with the measured offline objects by minimizing ΔR. The same explanation can be used to motivate the differences in efficiency for the $p_{T,\ell\ell}$ distribution since events with a low $\Delta\phi_{\ell\ell}$ usually correspond to high $p_{T,\ell\ell}$.

In the $m_{\ell\ell}$ distribution in Figure 8c, however, there is a more concerning difference between the original new proposal and the reconstruction: the reconstruction shows a drop in efficiency when going lower than 60 GeV (as expected since this is requested) which is not clear in the original proposal. There is no immediate reason why this 60 GeV-drop doesn't happen for the new trigger proposal, and this should be looked at by the relevant experts.

Hereafter one can try to optimize the trigger by tweaking the L1 $\Delta\phi_{\ell\ell}$ cut. Since here no background events are considered, there is no way in knowing how much the $\Delta\phi_{\ell\ell}$-cut can be lowered before the accepting rate gets too high. Therefore the event phase space is split up in three regions based on the $p_{T,\ell\ell}$-value:

- The low-$p_{T,\ell\ell}$ region: $p_{T,\ell\ell} < 20\,\text{GeV}$
- The intermediate region: $20 \leqslant p_{T,\ell\ell} < 40\,\text{GeV}$
- The high-$p_{T,\ell\ell}$ region: $p_{T,\ell\ell} \geqslant 40\,\text{GeV}$

The objective is then to look at which point the new trigger proposal still increases in low-$p_{T,\ell\ell}$ regions (which is where an increase is desirable) and intermediate regions. At some point this increase in these regions will stop and only in high-$p_{T,\ell\ell}$ regions the efficiency will increase, which is quite useless. In this way a lower limit can be estimated. In addition to tweaking the Level-1 $\Delta\phi_{\ell\ell}$ also an offline $\Delta\phi_{\ell\ell}$ cut was added to the new trigger proposal before calculating the efficiency in order to cut away the transition region as well as an invariant mass cut of $m_{\ell\ell} \geqslant 72\,\text{GeV}$.

The results can be found in Table 1. In this table strict inequalities are used for the $\Delta\phi_{\ell\ell}$-cuts as opposed to the implementation of the new trigger proposal. Since an L1 $\Delta\phi_{\ell\ell}$ measurement has an uncertainty of 0.1 rad, keeping events with $\Delta\phi_{\ell\ell} > 2.4$ corresponds to keeping events with $\Delta\phi_{\ell\ell} \geqslant 2.5$. From this table it is clear that there is little use in going any lower than an L1 cut of 2.1 rad.

Table 1: Efficiency increases for different $p_{T,\ell\ell}$ regions for different Level-1 $\Delta\phi_{\ell\ell}$ cuts including the corresponding offline $\Delta\phi_{\ell\ell}$ cut.

$\Delta\phi_{\ell\ell}^{\text{L1}} >$ [rad]	$\Delta\phi_{\ell\ell} >$ [rad]	Efficiency increase			
		$p_{T,\ell\ell} < 20\,\text{GeV}$	$20 \leqslant p_{T,\ell\ell} < 40\,\text{GeV}$	$p_{T,\ell\ell} \geqslant 40\,\text{GeV}$	Overall
2.7	2.85	0.14	0.11	0.01	0.11
2.4	2.55	0.18	0.14	0.02	0.14
2.1	2.25	0.19	0.16	0.03	0.16
2.0	2.15	0.19	0.16	0.04	0.16
1.9	2.05	0.19	0.16	0.04	0.16
1.4	1.55	0.19	0.17	0.07	0.17

4 Conclusion

When trying to measure the weak mixing angle with high accuracy, it is interesting to look at dileptonic decays of the Z-boson with a high rapidity of the reconstructed system. As could be concluded from Figure 4, these are usually events where one central and one forward electron are produced. In order to be able to optimize the acceptance of events which are significant to high precision measurements of the weak mixing angle, a trigger on central-forward events is constructed.

During the first two runs of the LHC, the ATLAS trigger solely triggered the CF-events on properties concerning the central electron, while exerting two offline cuts on the transverse momentum of both electrons. The proposal for run 3 now consists of lowering the p_T-cut on the central electron, in order to accept more events, and then, to be able to deal with the increase in rate, further trigger on properties concerning the dileptonic system among which an online $\Delta\phi_{\ell\ell}^{L1}$-cut of 2.5 rad and an online $m_{\ell\ell}^{L1}$-cut of 60 GeV.

In section 3.1, this proposal was tested on Monte-Carlo simulated data for run 2 and compared to the old trigger. Since the new trigger proposal has a strong increase in efficiency at low-$p_{T,\ell\ell}$ regions, while performing worse at higher $p_{T,\ell\ell}$ regions (due to the $\Delta\phi_{\ell\ell}^{L1}$-cut), it is more interesting to combine both the run 3-proposal and the former trigger: either an event is accepted by the new proposal or by the old trigger. This ensured an overall efficiency gain of 12.5%.

In section 3.2, the new trigger proposal was reconstructed by matching the L1-objects to the corresponding offline objects by minimizing ΔR. When observing the efficiency of both the original and the reconstructed new trigger proposal for the distribution of the invariant mass $m_{\ell\ell}$ (Figure 8c), it was found that in the reconstruction the efficiency drops when going lower than 60 GeV (as is requested in the new trigger proposal), while this drop is not obvious in the original run 3 proposal. There is no immediate reason for this discrepancy, and the implementation of the original run 3 proposal should be looked at.

This reconstruction of the new trigger was used to tweak the online $\Delta\phi_{\ell\ell}$ cut. With the available information a lower limit on the online cut could be found and was determined to be 2.1 rad, as can be concluded from Table 1. Before proposing to lower the threshold from 2.5 rad to 2.1 rad, however, it still needs to be checked what the increase in rate is associated with this change.

Appendices

A Offline Distributions of Dynamical Properties

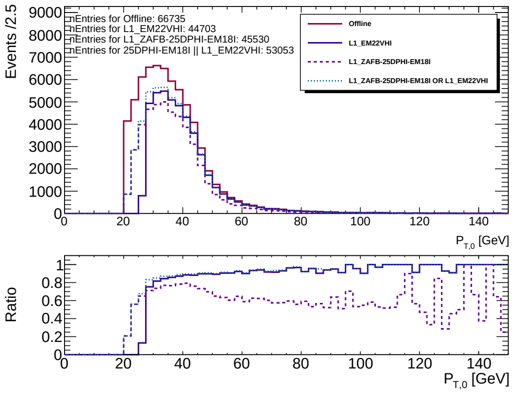

(a) $p_{T,0}$ distribution

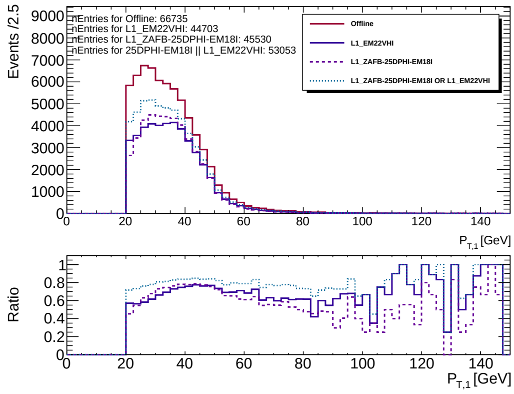

(b) $p_{T,1}$ distribution

Figure 9: Comparing the effects of the old and new L1 trigger on distributions of the transverse momenta of the individual electrons to the offline selection.

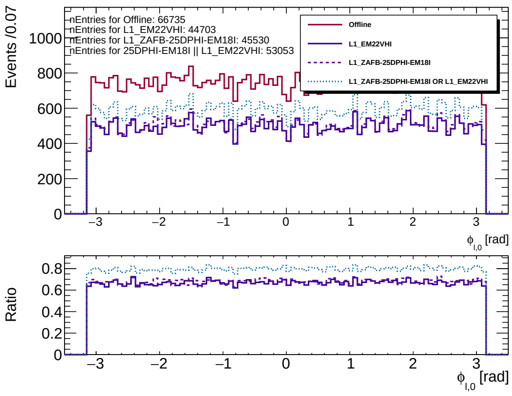

(a) $\phi_{\ell,0}$ distribution

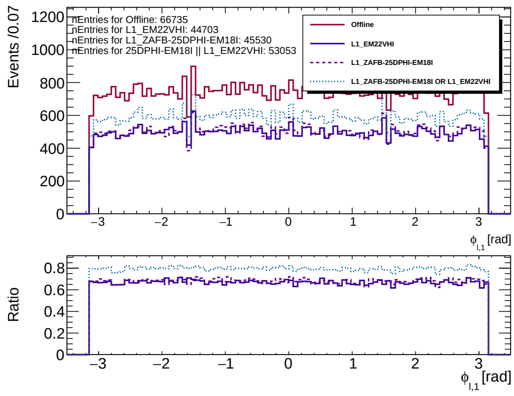

(b) $\phi_{\ell,1}$ distribution

Figure 10: Comparing the effects of the old and new L1 trigger on distributions of the azimuthal angles of the individual electrons to the offline selection.

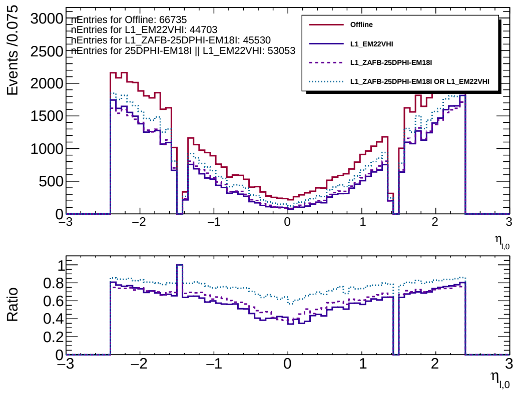

(a) $\eta_{\ell,0}$ distribution

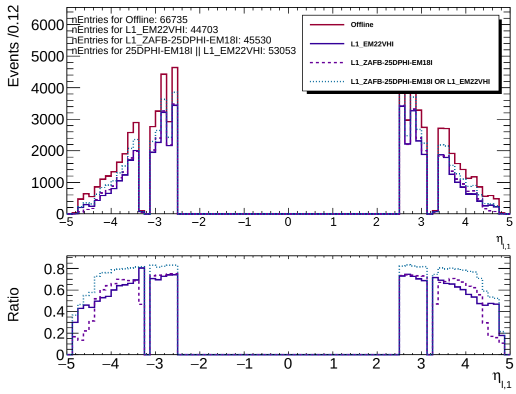

(b) $\eta_{\ell,1}$ distribution

Figure 11: Comparing the effects of the old and new L1 trigger on distributions of the pseudorapidities of the individual electrons to the offline selection.

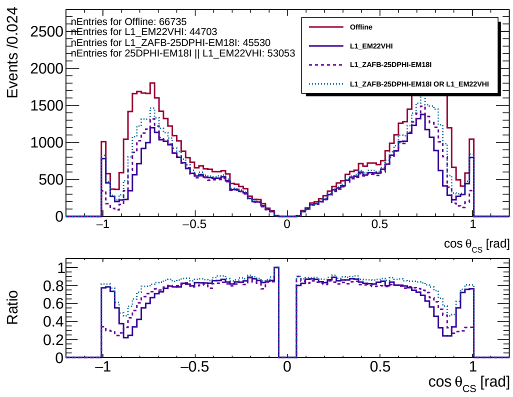

(a) $\cos\theta_{\mathrm{CS}}$ distribution

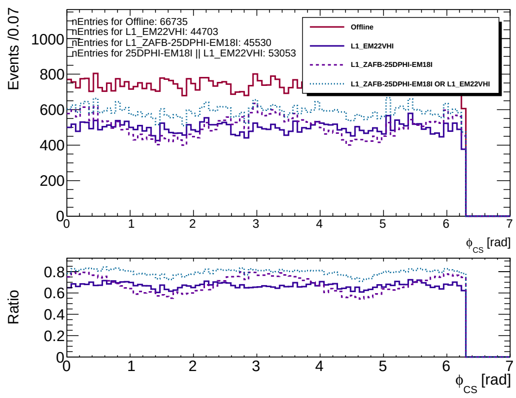

(b) ϕ_{CS} distribution

Figure 12: Comparing the effects of the old and new L1 trigger on the angular distributions measured in the Collins-Soper frame to the offline selection.

B L1 Distributions of Dynamical Properties

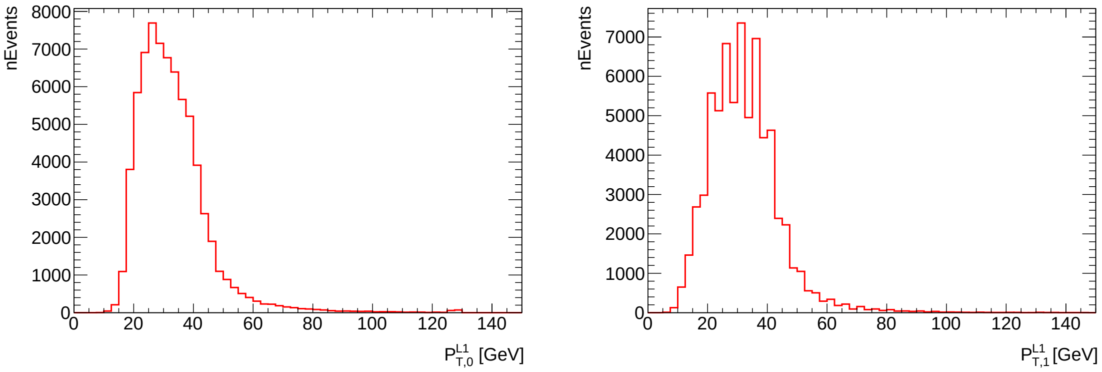

(a) $p_{T,0}^{L1}$ distribution

(b) $p_{T,1}^{L1}$ distribution

Figure 13: Distrubtions of the transverse momenta of the individual leptons at the Level-1 measurements.

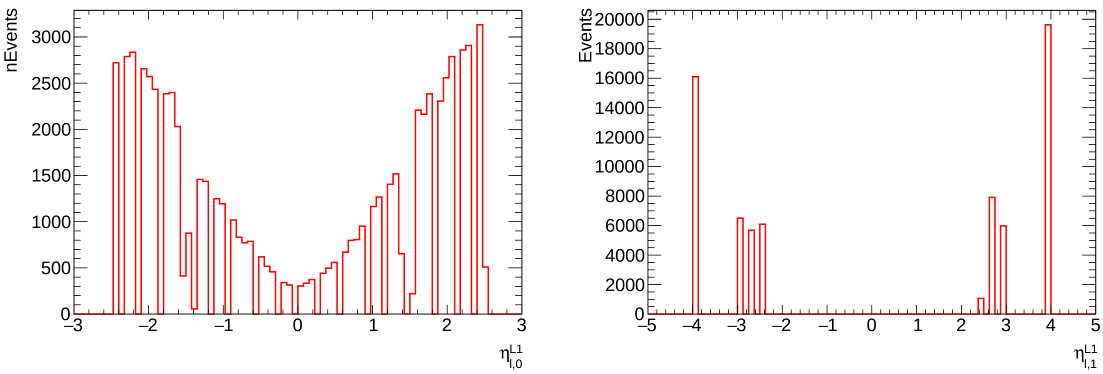

(a) $\eta_{\ell,0}^{L1}$ distribution

(b) $\eta_{\ell,1}^{L1}$ distribution

Figure 14: Distrubtions of the pseudorapidities of the individual leptons at the Level-1 measurements.

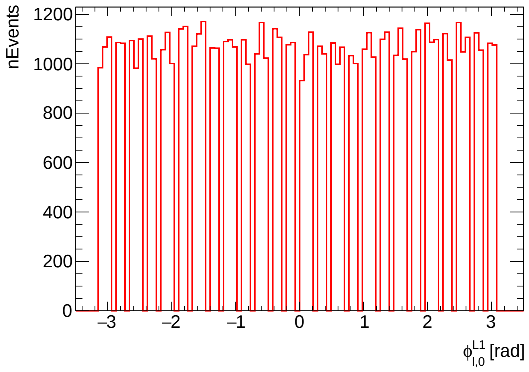

(a) $\phi_{\ell,0}^{L1}$ distribution

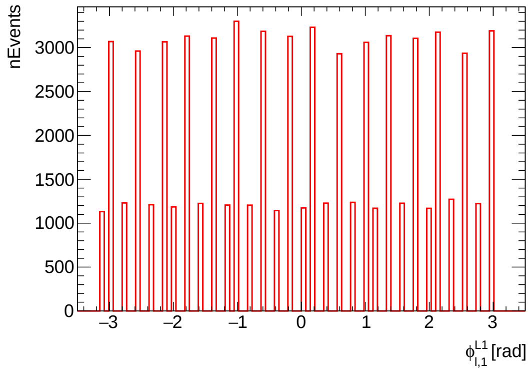

(b) $\phi_{\ell,1}^{L1}$ distribution

Figure 15: Distrubtions of the azimuthal angles of the individual leptons at the Level-1 measurements.

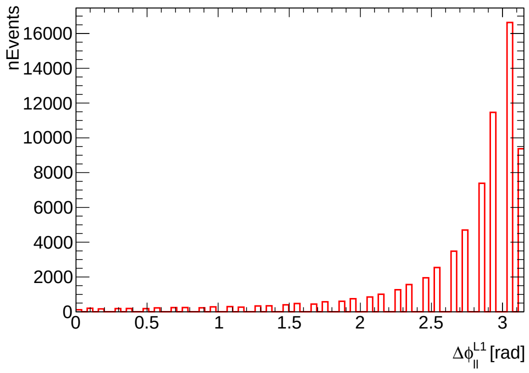

(a) $\Delta\phi_{\ell\ell}^{L1}$ distribution

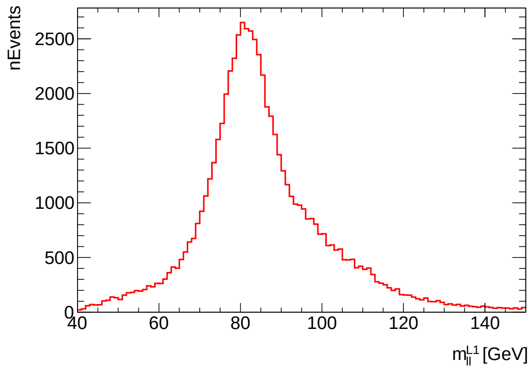

(b) $M_{\ell\ell}^{L1}$ distribution

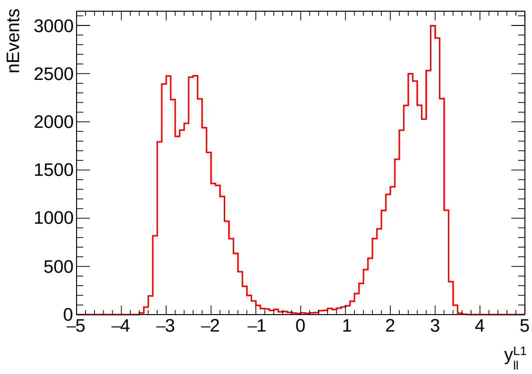

(c) $y_{\ell\ell}^{L1}$ distribution

Figure 16: Distrubtions of the dileptonic properties at the Level-1 measurements.

References

[1] *"About the ATLAS Experiment"*, https://atlas.cern/discover/about, last retrieved on September 17, 2019

[2] *"Trigger and Data Acquisition System"*, https://atlas.cern/discover/detector/trigger-daq, last retrieved on September 17, 2019

[3] F. Mandl & G. Shaw, *"Quantum Field Theory"*, second edition, Wiley, 2010

[4] Gfitter, http://project-gfitter.web.cern.ch/project-gfitter/, last retrieved on September 10, 2019

[5] The ATLAS Collaboration, *"Measurement of the effective leptonic weak mixing angle using electron and muon pairs from Z-boson decay in the ATLAS experiment at* $\sqrt{s} = 8$ *TeV"*, ATL-CONF-2018-037, July 11, 2018

[6] The ATLAS Collaboration, *"Measurement of the angular coefficients in Z-boson events using electron and muon pairs from data taken at* $\sqrt{s} = 8$ *TeV with the ATLAS detector"*, arXiv: 1606.00689v1 [hep-ex], June 2, 2016

[7] M. Thomson, *"Modern Particle Physics"*, Cambridge University Press, 2013